

# GigaScience

## Qiber3D - an open source software package for the quantitative analysis of networks from 3D image stacks

--Manuscript Draft--

<b>Manuscript Number:</b>	GIGA-D-21-00182	
<b>Full Title:</b>	Qiber3D - an open source software package for the quantitative analysis of networks from 3D image stacks	
<b>Article Type:</b>	Technical Note	
<b>Funding Information:</b>	national breast cancer foundation (PF-16-004)	Dr Laura J Bray
	cancer australia (1159637)	Dr Laura J Bray
	leukemia foundation of australia (1159637)	Dr Laura J Bray
<b>Abstract:</b>	<p><b>Background :</b> Optical slice microscopy is commonly used to observe cellular morphology in 3D tissue culture, for example, the formation of cell-derived networks in angiogenesis models. Morphometric quantification of these networks is essential to study the cellular phenotype. Commonly these measurements are performed on 2D projections of the image stack and relevant information in 3D is missed. Currently, available 3D image analysis tools rely on manual interactions with the software and are not feasible for large datasets.</p> <p><b>Findings :</b> Here we present Qiber3D, an open-source image processing toolkit. The software package comprises all essential image analysis procedures required for image processing, from the raw image to the quantified data. Optional pre-processing steps can be switch on/off depending on the input data condition. Two reconstruction algorithms are offered to meet the requirements for a wide range of network types. Furthermore, Qiber3D's rendering capabilities enable the user to inspect each step of the workflow interactively to ensure the creation of an optimal workflow for each application.</p> <p><b>Conclusions :</b> Qiber3D is implemented as Python package and its source code is freely available at <a href="https://github.com/theia-dev/Qiber3D">https://github.com/theia-dev/Qiber3D</a> . The building block principle makes it suitable to analyse a variety of structures, such as vascular networks, neuronal structures, or scaffolds from numerous input formats. While Qiber3D can be used interactively in the Python console, it is aimed at automation to process large image datasets efficiently.</p>	
<b>Corresponding Author:</b>	Anna Jaeschke Queensland University of Technology Kelvin Grove, QLD AUSTRALIA	
<b>Corresponding Author Secondary Information:</b>		
<b>Corresponding Author's Institution:</b>	Queensland University of Technology	
<b>Corresponding Author's Secondary Institution:</b>		
<b>First Author:</b>	Anna Jaeschke	
<b>First Author Secondary Information:</b>		
<b>Order of Authors:</b>	Anna Jaeschke	
	Hagen Eckert	
	Laura J Bray	
<b>Order of Authors Secondary Information:</b>		
<b>Additional Information:</b>		
<b>Question</b>	<b>Response</b>	

<p>Are you submitting this manuscript to a special series or article collection?</p>	<p>No</p>
<p><b>Experimental design and statistics</b></p> <p>Full details of the experimental design and statistical methods used should be given in the Methods section, as detailed in our <a href="#">Minimum Standards Reporting Checklist</a>. Information essential to interpreting the data presented should be made available in the figure legends.</p> <p>Have you included all the information requested in your manuscript?</p>	<p>Yes</p>
<p><b>Resources</b></p> <p>A description of all resources used, including antibodies, cell lines, animals and software tools, with enough information to allow them to be uniquely identified, should be included in the Methods section. Authors are strongly encouraged to cite <a href="#">Research Resource Identifiers</a> (RRIDs) for antibodies, model organisms and tools, where possible.</p> <p>Have you included the information requested as detailed in our <a href="#">Minimum Standards Reporting Checklist</a>?</p>	<p>Yes</p>
<p><b>Availability of data and materials</b></p> <p>All datasets and code on which the conclusions of the paper rely must be either included in your submission or deposited in <a href="#">publicly available repositories</a> (where available and ethically appropriate), referencing such data using a unique identifier in the references and in the “Availability of Data and Materials” section of your manuscript.</p> <p>Have you have met the above requirement as detailed in our <a href="#">Minimum</a></p>	<p>Yes</p>

[Standards Reporting Checklist?](#)



## TECHNICAL NOTE

# Qiber3D - an open source software package for the quantitative analysis of networks from 3D image stacks

Anna Jaeschke<sup>1,2,\*</sup>,<sup>†</sup>, Hagen Eckert<sup>3,†</sup> and Laura J. Bray<sup>1,2,4</sup>

<sup>1</sup>Centre for Biomedical Technologies, Queensland University of Technology (QUT), Kelvin Grove, Australia and <sup>2</sup>School of Mechanical, Medical and Process Engineering, Science and Engineering Faculty, Queensland University of Technology (QUT), Brisbane, Australia and <sup>3</sup>Department of Mechanical Engineering and Materials Science, Duke University, Durham, NC, USA and <sup>4</sup>ARC Training Centre for Cell and Tissue Engineering Technologies, Queensland University of Technology (QUT), Kelvin Grove, Australia

\*anna.jaeschke@connect.qut.edu.au

<sup>†</sup>Contributed equally.

## Abstract

**Background:** Optical slice microscopy is commonly used to observe cellular morphology in 3D tissue culture, for example, the formation of cell-derived networks in angiogenesis models. Morphometric quantification of these networks is essential to study the cellular phenotype. Commonly these measurements are performed on 2D projections of the image stack and relevant information in 3D is missed. Currently, available 3D image analysis tools rely on manual interactions with the software and are not feasible for large datasets. **Findings:** Here we present Qiber3D, an open-source image processing toolkit. The software package comprises all essential image analysis procedures required for image processing, from the raw image to the quantified data. Optional pre-processing steps can be switch on/off depending on the input data condition. Two reconstruction algorithms are offered to meet the requirements for a wide range of network types. Furthermore, Qiber3D's rendering capabilities enable the user to inspect each step of the workflow interactively to ensure the creation of an optimal workflow for each application. **Conclusions:** Qiber3D is implemented as Python package and its source code is freely available at <https://github.com/theia-dev/Qiber3D>. The building block principle makes it suitable to analyse a variety of structures, such as vascular networks, neuronal structures, or scaffolds from numerous input formats. While Qiber3D can be used interactively in the Python console, it is aimed at automation to process large image datasets efficiently.

**Key words:** morphometric quantification; confocal imaging; image processing; vascular networks; fibrous networks; neurons

## Background

The process of angiogenesis, the development of new blood vessels from the existing vasculature, is the center of numerous research questions. The evaluation of the processes and factors involved in vessel formation, maturation and remodeling is essential for a better understanding of normal development and angiogenesis-related disease stages [1, 2]. *In vitro* angiogenesis models aim towards replicating the formation of vascular-like networks in the laboratory [2]. Optical slice microscopy is commonly used to follow vessel formation in *in vitro* angiogenesis models [3]. Thereby, multiple images are acquired across different

positions in the z-plane throughout the specimen capturing the cell morphology in 3D [3]. The vascular phenotype can be assessed by qualitative observation or by morphometric quantification of fiber length, number of fibers, cross-sectional area or volume as well as branching [2]. The characterization of the morphological phenotype is an essential tool to study cellular responses. Currently, morphometric quantification usually relies on 2D projections, often maximum intensity projections, of the 3D images. However, 2D quantification of 3D structures limits the accuracy of data obtained and results in the loss of relevant information in the third dimension [4]. Consequently, there is a need for quantification

Compiled on: June 24, 2021.

Draft manuscript prepared by the author.

tools of 3D image files that can be adapted to various areas of research studying networks composed of elongated or fiber-like structures.

Computational approaches exist to visualize and investigate cell morphology in 2D and 3D. Proprietary software packages, for example Amira™ (ThermoFisher Scientific) [5], Imaris (Oxford Instruments) or Metamorph® (Molecular Devices) are capable of 3D, 4D and 5D image processing and analysis. However, proprietary software often acts as a black box at various stages of the analytic workflow. While the documentation usually covers the basic components of a function, the actual implementation is not revealed. Often, the software packages are designed to be standalone products complicating the integration with existing analysis protocols and programs. Furthermore, the licensing expenses limit accessibility to the software. Therefore, a multitude of free-to-use image processing software packages have been developed. Many of these tools are widely extensible by the use of plugins [6, 7] and the source code is often fully accessible (open-source). The programs that are available for 3D image processing tasks, are often focused on the visualization of the 3D data [6, 8, 9].

Available 3D quantification protocols often combine existing software packages, and commonly require manual handling, at least for parts of the image analysis workflow [10, 11, 12]. Besides carrying the risk of user-based subjectivity, it also limits the throughput of samples for experiments with large image datasets. In some cases, switching between multiple existing software packages is necessary [12], making the image processing time- and resource-consuming and therefore, again, not feasible for large data sets.

Here we present `Qiber3D` an open-source software package for morphometric quantification of networks from 3D image stacks. `Qiber3D` combines the required tools for a complete analytical workflow, from the raw image to final measured values. The core method of `Qiber3D` for the reconstruction of networks is based on thinning. While this approach covers many applications, for example vascular-like networks or scaffolds, we offer the `kimimaro` implementation of the Tree-structure Extraction Algorithm for Accurate and Robust skeletons (TEASAR) [13, 14] as an alternative skeletonization method. With the implementation of two reconstruction modes, `Qiber3D` is usable for the quantification of a variety of fibrous networks from image stacks.

`Qiber3D` generates a graph representation of a network based on various input formats. Interactive inspection of the network at each step of the workflow assists with the optimization of image processing parameters. The extracted quantitative morphometric data can be exported in a multitude of options to provide broad compatibility with other software. The implementation as an open-source Python package creates a highly customizable program that is suitable for image analysis automation and tight integration into existing workflows. By design, `Qiber3D` is suitable for applying general batch distribution approaches to be used on high-performance computing (HPC) clusters enabling high-throughput image analysis for large datasets.

## Findings

### Implementation

Here we present an image processing toolkit that integrates the steps for 3D morphometric quantification of cellular or fibrous networks from image stacks. The general workflow of `Qiber3D` is depicted in Fig 1. Optional steps can be included or excluded from the image processing pipeline depending on the user's requirements. Thereby, the toolkit can be customized allowing `Qiber3D` to be applied on raw as well as preprocessed images from a vari-

ety of sources. `Qiber3D` is developed as a command line tool enabling smooth integration into existing workflows as well as automated, high-throughput images analysis. However, visualization is achieved using `vedo`, allowing the user to interact with the image output at different stages during image processing.

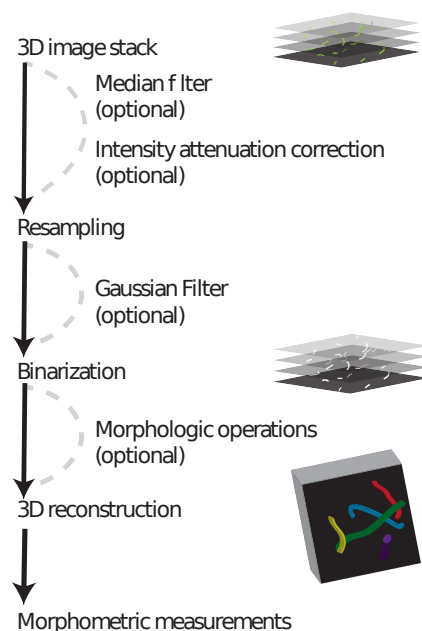


**Figure 1.** `Qiber3D`'s workflow combines the required image processing steps for 3D morphometric quantification of networks. Optional tools are provided to cover a range of input images.

**Image generation and acquisition.** As experimental image stacks reach sizes of well over 500 MB, we included a method to create *synthetic* network images. This allows for proper unit tests of the source code without the need to download large datasets. Moreover, synthesizing an example data set provides full control over the input dimensions and enables a direct comparison with the expected output. We utilized this *synthetic* network in the unit tests and alongside an image stack of a microvascular network to demonstrate the analytic steps of `Qiber3D`.

**Read image data.** Confocal images are usually acquired using commercial imaging platforms and the image files are saved in a proprietary file format, containing the metadata. `Qiber3D`'s support for multi-dimensional image formats is based on PIMS<sup>1</sup> (Python Image Sequence). This choice allows the use of essential image formats like TIFF-stacks as well as proprietary file formats from microscope vendors like Leica, Nikon, Olympus, and Zeiss as input. Physical size information (the voxel size) and, for multi-channel images, the channel of interest for network reconstruction is provided upon image loading or set as configuration variable for automated workflows. For some file formats, `Qiber3D` is able to extract the required metadata directly from the input file.

**Median filter (optional).** The primary purpose of the 3D median filter, also known as the despeckle filter, is the removal of speckles and extrema. The value of each voxel is replaced by the median of its surrounding voxels. By default, a three voxels wide neighborhood is used. However, this size can be modified in the configuration

<sup>1</sup> <https://github.com/soft-matter/pims>

depending on the noise present in the image.

**Intensity attenuation correction (optional).** In 3D confocal images, light absorption can cause a decrease in signal intensity in slices located deeper into the sample. An exponential curve is fitted to the average intensities  $I_A$  in each of the slices to their physical stack position  $z$  to correct for this intensity attenuation (Fig. 2).

$$I_A = a \exp(bz) \quad (1)$$

The optimal parameters  $a$  and  $b$  for the intensity correction are determined using a non-linear least-squares fit.

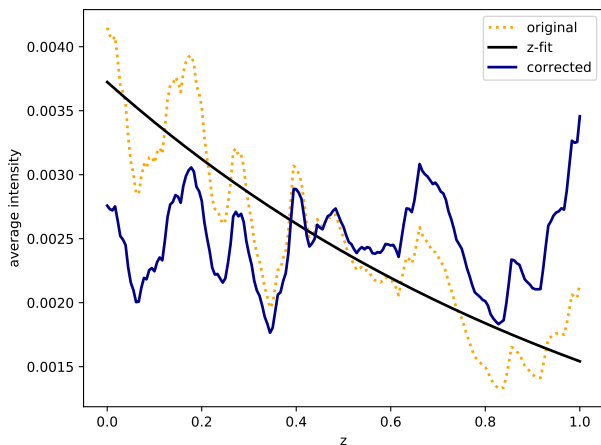


**Figure 2.** Intensity attenuation correction in the example image of the microvascular network. Yellow - original signal. Blue - corrected signal. Black - intensity fit.

**Resampling to an isotropic voxel size.** Commonly, the  $x/y$  resolution of image stacks differs from the resolution along the  $z$ -axis. As a cubic voxel size is beneficial to optimize the subsequent image processing steps, the  $z$ -axis of the image is resampled to the same resolution as the  $x/y$  plane using a third order spline interpolation.

**Gaussian filter (optional).** The image stack is blurred with a Gaussian filter simultaneously in all three dimensions to minimize the effect of noise on the image segmentation by reducing sharp differences between neighboring pixels. Application of the Gaussian filter reduces the noise level and imaging artifacts significantly. This results in more consistent boundaries of the features of interest.

**Binarization.** The grayscale image is reduced to a binary representation to locate the boundaries of the structures and to label the segments. All voxels that are equal to or greater than a threshold are set to True and all others to False. A dynamic threshold calculation for each stack is performed using the Otsu method permitting an automated workflow. The unsupervised, nonparametric method tries to maximize the separability of the resultant classes (exactly two in the binary image), by utilizing the zeroth- and first-order moments of the histogram [15].

**Morphologic operations (optional).** The obtained structures in the binarized image stack might not be perfectly solid, depending on the quality of the input data. A sequence of 3D erosion and dilation operations is performed to fill small holes and compact the segments' surface. This step also removes small islands caused by imaging artifacts.

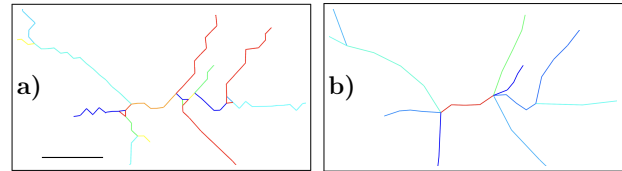


**Figure 3.** Network optimization. After thinning (a), the network is optimized by replacing tiny segments with more extensive structures and smoothing out voxel artifacts (b). Scale bar:  $12.3 \mu\text{m}$  (10 voxel)

**Reconstruction by thinning (default).** The default network reconstruction approach is based on thinning, a morphological operation to remove selected foreground pixels from binary images. Initially, the image stack is distance transformed and every foreground (*True*) voxel in the stack is assigned the shortest Euclidean distance to a background (*False*) voxel. Subsequently, the Lee-Kashyap algorithm [16] is applied to extract the medial axis, and the binary image is reduced to its skeleton. The remaining foreground voxels, the skeleton, are modeled as a graph, defined by vertices that are connected by edges. Each foreground voxel represents a vertex, and connecting edges are formed between neighboring voxel. A radius is assigned to each vertex based on the earlier distance transformation. To form *Segments* (see below for details), the graph is reduced to contain only vertices that represent end and branch points.

Distinctive edges are often formed along with branch points, sharp bends, or on the network's rim. Such edges occur between vertices that are direct neighbors and the resulting path is particularly jagged (Fig 3 a). This resolution artifact results in an overestimation of the fiber length and volume and an inflated branch point count. To mitigate these drawbacks, edges that are shorter than six voxel are merged with larger neighbors or removed if isolated and each edge is interpolated using a cubic spline (Fig. 3 b). New points are generated at a rate of approximately one point every ten voxel for edges longer than 50 voxels.

**Reconstruction with TEASAR (alternative).** Initially, the TEASAR method aimed to generate organ centerlines from 3D imaging generated by MRI, or CT scans [13, 14]. It has been used in a variety of applications, from pore networks in clay rocks [17, 18], to neuronal networks [19, 20] since. `Qiber3D` incorporates the `kimimaro`<sup>2</sup> implementation of the TEASAR algorithm that was developed to skeletonize neurons. For processing networks that resemble neuronal structures, that is branching of structures (dendrites) from a cell body (soma), the use of this method is recommended over the thinning-based reconstruction. The output of the skeletonization step is a connected graph, from which we extract the quantitative measurements of the network.

**Morphometric measurement.** In `Qiber3D` the reconstructed network is represented in a hierarchical structure (Fig. 4). We use the terms *Network*, *Fiber*, and *Segments* to describe the components of the reconstruction. Note that these expressions are purely used conceptually to label `Qiber3D`'s output and that the terms might not refer to the actual structure. A *Fiber* might be a real fiber, an elongated cell, or another object depending on the application.

The largest entity is the *Network*, which represents the entirety of the structure. It is composed of a collection of *Fibers*, that are formed by connected *Segments*, the smallest elements. A *Segment* is described by a collection of sorted points stored along the corresponding radius. The vertices between the points are interpreted as truncated cones. *Segments* end when they reach a branch point (grey points, Fig. 4). Therefore, *Segments* themselves are never branched. A branch point belongs to all *Segments* that it connects.

<sup>2</sup> <https://github.com/seung-lab/kimimaro>

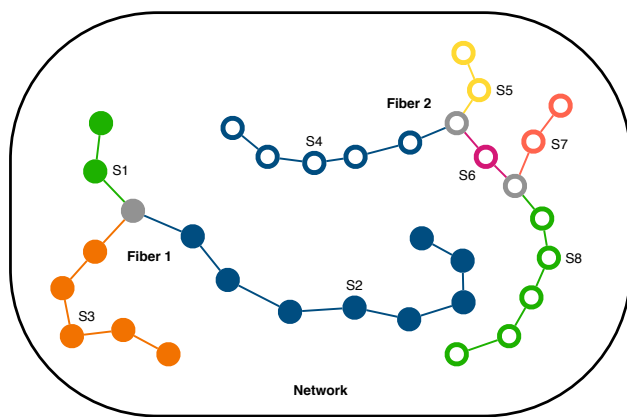


**Figure 4.** Qiber3D's hierarchical structure. Segments S1–S3 generate Fiber 1 (filled points) and segments S4–S8 Fiber 2 (hollow points), forming the Network. Branch points are colored in gray.

Each element, on the different hierarchical levels, is defined by a unique identifier and several quantitative properties, for example, the volume or the average radius. The average radius can be misleading considering that the distance between the points forming an element can be non-uniform resulting in a skewed measurement. Therefore, we included the notion of a length-weighted cylindrical radius and return the radius of a cylinder with the same volume and length as the element of interest. While the modelling of the volume as overlapping truncated cones is sufficient in most cases, an improved volume estimation can be obtained from the rasterized network. As the start and endpoint of a Fiber within a given 3D image stack is interchangeable, the directional data is analysed based on the assumption that all Fibers are pointing upwards (positive z-axis). Depending on the application, Fibers can be convoluted and the orientation of the Segments can be more meaningful in some cases. In both cases, the orientation of each element is described using the azimuth and altitude regarding a half-sphere.

For the Network additional measurements, like the number of Fibers, Segments and branch points, or the bounding box volume, are provided. The Network object also stores the relevant metadata of the input.

**Visualization.** Qiber3D uses `vedo`, a lightweight python module, that is based on `VTK` and `numpy` [21], to visualize the network in 3D. The embedded rendering capability allows the users to quickly inspect a network by rotating the camera view and zoom into regions of interest. A linked view of the different reconstruction steps and the resulting skeleton enables the user to examine them in relation to each other. The network's color can be customized to represent different properties of the network, such as fiber length, volume, or average radius. In addition to the interactive visualization, 3D views can be exported as static images or animations.

**Import/export.** As interoperability is an essential goal of the Qiber3D toolkit, a wide variety of import and export options is paramount. Besides loading 3D image stacks to create the Network object, it can be built from files describing the network. Qiber3D supports the MicroVisu3D format `.mv3d`, traditionally used for vascular networks, as well as the `.swc` and the `.ntr` format, popular for neuronal networks.

The internal representation of the Qiber3D network can be stored as a binary NumPy file (`.npz`) that allows for fast loading of the reconstructed network into the software. Easy visualization in web applications, and the import into specialized rendering software like `Blender` is achieved by saving the 3D representation as a collection of truncated cones in the `.x3d` file format. Moreover, Qiber3D supports several human-readable formats. The spatial data of the reconstructed network can be exported as `.mv3d`, `.swc` and `.csv` files.

When exporting to a `.json` or Microsoft Excel `.xlsx` file format, the complete set of metadata and calculated properties is included. Furthermore, the network can be exported as a 3D `.tiff` image stack.

## Results

To provide a comprehensive overview of the features, Qiber3D was applied to the synthetic example image as well as two experimental data sets, an *in vitro* microvascular network and a neuron that was reconstructed elsewhere.

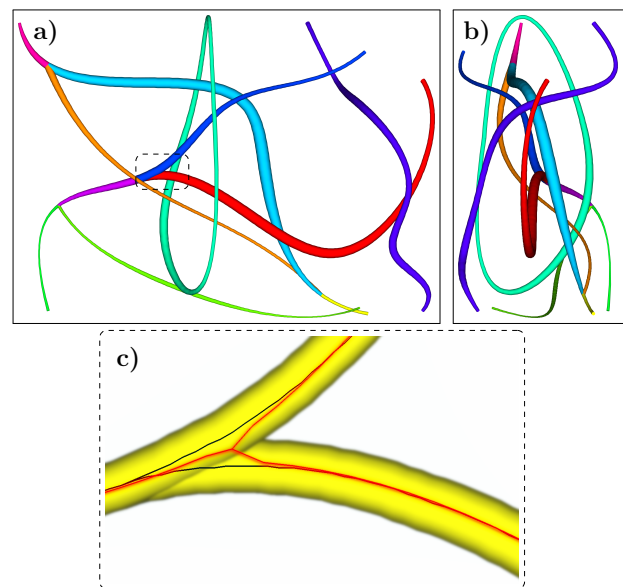


**Figure 5.** Synthetic network example with a) view on the x/y-plane and b) view on the z/y-plane. c) A branch point of the synthetic network with the original (black) and reconstructed (red) centerlines.

### Synthetic example image

The output of the synthetic example image is presented in Fig. 5 and Suppl. Movie 1<sup>3</sup>. The example network was visualized in 3D and the segments composing the fibers were observed (Fig. 5 a). The measurements of the network reconstructed with Qiber3D were in agreement with the input data (Tab. 1). Interestingly, the branch points of the fibers were slightly displaced (Fig. 5 c) without affecting the measured total volume of the network (Tab. 1). This discrepancy is due to the thickness of the fibers concealing the original merging points during reconstruction.

**Table 1.** Comparison of the synthetic network with the output of Qiber3D after reconstruction.

	synthetic network	Qiber3D output
Number of fibers	4	4
Total length [ $\mu\text{m}$ ]	1141.44	1120.84
Total Volume [ $\mu\text{m}^3$ ]	4688.67	4665.62
Average radius [ $\mu\text{m}$ ]	0.94	0.96
Cylinder radius [ $\mu\text{m}$ ]	1.14	1.15

<sup>3</sup> <https://figshare.com/s/11a68052c2fb564b74ac>

### Microvascular network

Qiber3D was used to analyze a confocal image of a network derived from microvascular cells grown *in vitro* (Fig. 6 a).

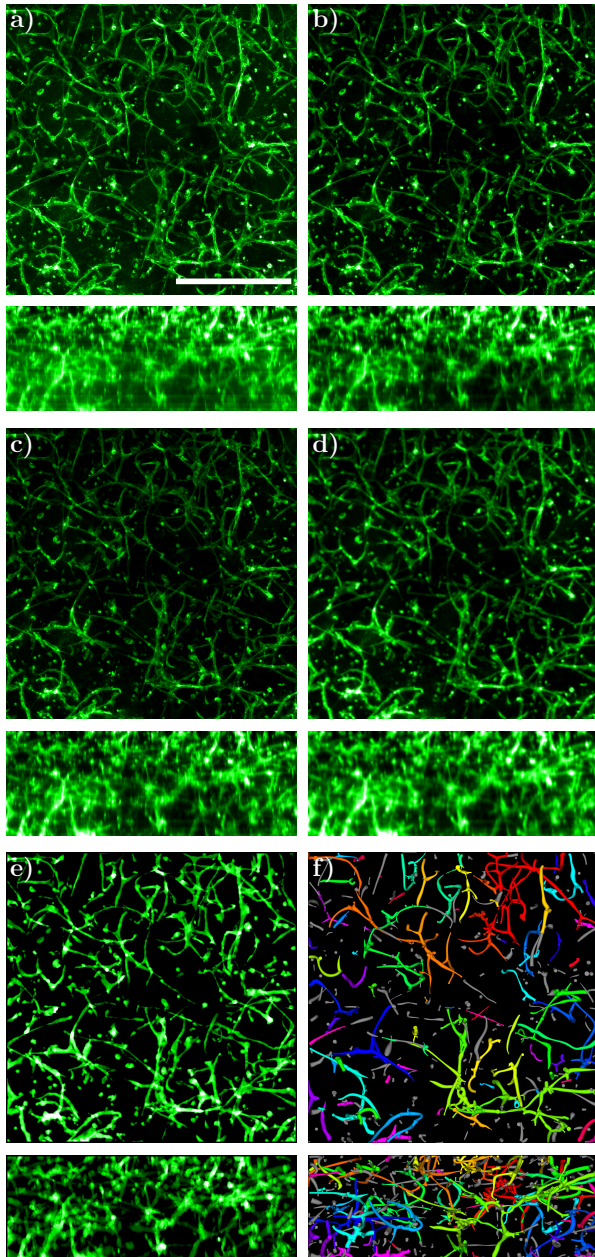


**Figure 6.** Qiber3D's image processing workflow. An image of each step is shown as a average intensity projection along the z-axis (upper panels) and along the x-axis (lower panels). a) Raw image. Scale bar: 500  $\mu\text{m}$ . b) Image after median filter. c) Image corrected for intensity attenuation (z-drop correction). d) Image after Gaussian blur and surface compacting. e) Binarized image. f) Reconstructed network.

The analysis was performed including all optional procedures of the workflow (Fig. 6). The application of the median filter resulted in a clearer image with fewer extrema (Fig. 6 b). Upon correction of the intensity attenuation, the distribution of signal was found more equal along the z axis (compare Fig. 6 b and c, lower panels). The quantitative observation was confirmed by the distribution of the mean signal intensity slice along the z axis before (Fig. 2, blue line) and after (Fig. 2, orange line) the correction step. If the z-drop correction was switched off, the vessels in the lower part of the image were lost after reconstruction of the network (Suppl. Fig. 1 b,

d-f). Following the intensity attenuation correction, a Gaussian filter resulted in noise reduction and smoothing of the boundaries (Fig. 6 d). After pre-processing the image using the optional filters, image segmentation was performed and morphological operations were applied to the binary image (Fig. 6 e). Omitting the morphological operations prior to reconstruction, resulted in the presence of numerous small particles that were not connected to the network ('islands') (Suppl. Fig. 1 c-e). Finally, the skeleton of the microvascular network was successfully reconstructed from the 3D image stack (Fig. 6 f, Suppl. Movie 2<sup>4</sup>). Each step was also visualized interactively while processing the input image or can be compared together afterwards (Suppl. Movie 3<sup>5</sup>). Removing the optional filter steps for the image of the microvascular-like network led to artifacts in the reconstructed network (Suppl. Fig. 1 b, e-f).

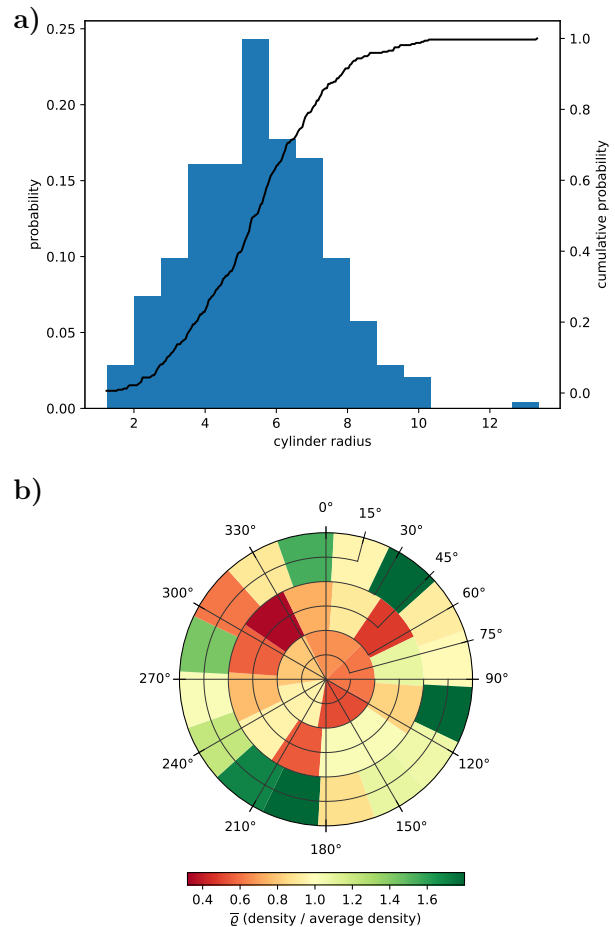


**Figure 7.** Graphical output of quantitative data in Qiber3D. a) Distribution of the cylinder radius of the fibers within the network. b) Orientation distribution of the fibers in 3D.

The distribution of network attributes can be visualized in Qiber3D in the form of a histogram. In Fig. 7 a the distribution of the cylinder radius is presented as an example. The fiber radii were normally distributed between 1 and 10  $\mu\text{m}$  with an average at 6.2  $\mu\text{m}$ . To visualize the directional distribution in 3D, we introduced a spherical histogram. In Fig. 7 b every bin represents a part of a half-sphere. The start point for every network fiber was considered to be at the center of the half-sphere. The segments of each fiber were averaged into a single vector that captures the fiber's dominant direction.

<sup>4</sup> <https://figshare.com/s/60967735e51d9cb03c7a>

<sup>5</sup> <https://figshare.com/s/81b04c0f61c83f4eb720>



**Table 2.** Comparison of the quantitative output from the NeuroMorph.org website, NLMorphology Viewer software, and Qiber3D.

	NeuroMorph	NLMorphology Viewer	Qiber3D
Branch points	30	30	30
Average Diameter [ $\mu\text{m}$ ]	1.09	na	1.38
Total length [ $\mu\text{m}$ ]	5097.48	5046.92	4991.83
Total Volume [ $\mu\text{m}^3$ ]	6362.05	6347.60	6288.30

As the surface area of the different bins of a half-sphere are not perfectly equal, the number of intersecting vectors were divided by the surface area of the bin. Furthermore, the fiber density of each bin was scaled using the average fiber density over the half-sphere to allow for a streamlined comparisons between multiple networks. The color scale indicates the scaled fiber density. For the microvascular network, the majority of fibers are located parallel to the x/y-axis (Fig. 7b).

Processing a 1 GB nd2 file with Qiber3D on an Intel Core i7-6700 machine with 16 GB RAM running a Windows 10 (64-bit) operation system took approximately 7.5 minutes. Manual analysing a similar image takes approximately 8.5 min, not considering the time to switch between various software packages [12]. While this is a slight decrease in processing time of one image, Qiber3D can be applied to numerous images without user interaction making it suitable to analyze large datasets. As Qiber3D is designed to run on a single CPU, running multiple processes of Qiber3D in parallel will accelerate the average image processing time for large datasets significantly. The use of build-in multiprocessing tools in Python enables straightforward implementation of parallel processing. For larger deployments on HPC clusters, tasks management using Message Passing Interface (MPI) for Python enables the analysis of vast image datasets. The implementation of Qiber3D as a Python package enables the smooth integration with other Python libraries to build customized tools that meet the requirements of varying computational environments, e.g. different HPC centers.

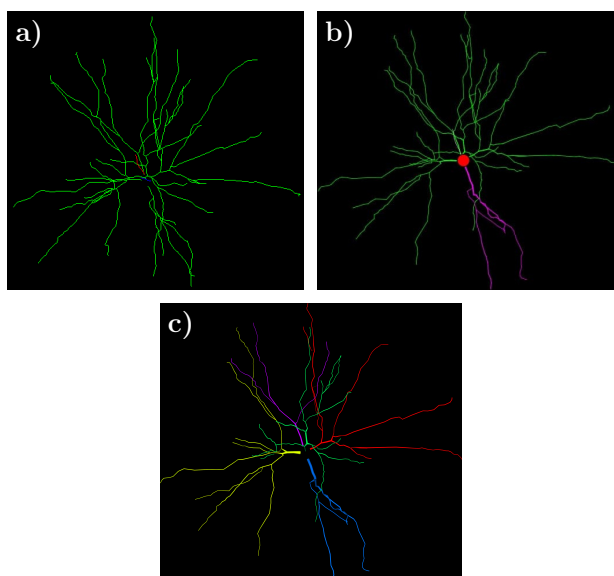


**Figure 8.** Visualization of the reconstructed neuron in a) NLMorphology Viewer, on b) NeuroMorph.org and c) with Qiber3D colored by fibers. Note, that the single neuron in this example represents exactly one fiber in Qiber3D

### Neuron morphology

We used Qiber3D to visualize and measure a reconstructed neuron from a red-necked wallaby [22]. The published *swc* file was obtained from NeuroMorph.org. We compared the 3D rendering of the neuron in Qiber3D with two other methods. The thickness of the

structures was clearly visible in the Qiber3D visualization (Fig. 8 c, Suppl. Movie 4<sup>6</sup>) similar to the image on NeuroMorph.org (Fig. 8 b). In contrast, the rendering with NLMorphology Viewer, a commonly used software tool to visualize neuron morphology, displayed all fibers with the same diameter (Fig. 8 b). The measurements from Qiber3D were in agreement with the published data on the NeuroMorph.org website as well as the output from NLMorphology Viewer (Tab. 2). The quantification of the total length in Qiber3D excludes the soma of the neuron. Therefore, the Qiber3D output was slightly lowered compared to the measurements with the other tools.

## Conclusion

Here we present Qiber3D, a toolkit to reconstruct and quantitatively analyze networks from 3D image stacks. The thinning-based core method of this software package is suitable to skeletonize a variety of networks from z-stack images. Additionally, Qiber3D offers skeletonization based on the kimimaro implementation of the TEASAR algorithm [13, 14]. By applying a building block principle, Qiber3D is developed to be highly customizable and adaptable for a variety of applications. Qiber3D can also be used in conjunction with other software packages, and integrated into existing analysis pipelines. The embedded visualization capability allows for the inspection of each image processing step to aid optimization of the image processing workflow. While the overall processing time is similar to manual processing, Qiber3D can be used fully hands-off to automate image analysis of numerous images. Moreover, running Qiber3D-based analysis on high performance computing clusters makes it suitable for high-throughput processing. In summary, Qiber3D is a versatile 3D image analysis toolkit that is accessible for a wide range of research questions.

## Methods

### Cell culture

Prostate microvascular cells (PrMECs) were obtained from ScienCell™ (Australian Biosearch, Wangara, WA, Australia) and expanded in endothelial cell medium (ECM) (Australian Biosearch, Wangara, WA, Australia). Cancer-associated fibroblasts (CAFs) were kindly provided by the Prostate Cancer Research Group, Department of Anatomy and Developmental Biology, Monash University [23]. The fibroblasts were cultured in RPMI 1640 media (no phenol red) (Gibco, ThermoFisherScientific, Scoresby, VIC, Australia) supplemented with 10 % fetal bovine serum (FBS) (Gibco, ThermoFisherScientific, Scoresby, VIC, Australia), 1 nM testosterone (Sigma-Aldrich, CastleHill, NSW, Australia), 10 ng mL<sup>-1</sup> FGF-2 (MiltenyiBiotec, MacquariePark, NSW, Australia), 100 U penicillin, and 100  $\mu\text{g mL}^{-1}$  streptomycin (Gibco, ThermoFisherScientific, Scoresby, VIC, Australia). All cells were maintained at 37 °C in a humidified incubator containing 5 % CO<sub>2</sub>, with media changes every 2-3 days.

## Preparation of hydrogel cultures

3D co-cultures were obtained using hydrogels comprised of synthetic starPEG and maleimide-functionalised heparin as described previously [24, 25]. Briefly, PrMECs and CAFs were seeded into hydrogels at a density of  $6 \times 10^6$  and  $6 \times 10^5$ , respectively. Vascular endothelial growth factor (VEGF) (Peprotech, Lonza, MountWaverly, VIC, Australia), human fibroblast growth factor 2 (FGF-2) and stromal cell-derived factor 1 (SDF-1) (MiltenyiBiotec, MacquariePark, NSW, Australia) were included into the gel at a concentration of  $5 \mu\text{g mL}^{-1}$  each. Additionally, 2 mol of RGD-SP (H<sub>2</sub>N-GCWGGRGDSP-CONH<sub>2</sub>) were added to the gel. A molar ration of starPEG to heparin-maleimide of 1:0.75 was used to obtain a stiffness of approximately 500 Pa (storage modulus). The starPEG-heparin hydrogels were maintained in ECM for 7 days at 37 °C in a humidified incubator containing 5 % CO<sub>2</sub>.

## Immunofluorescence of hydrogels

The cell-containing hydrogels were fixed in 4 % (v/v) paraformaldehyde (PFA) (Sigma-Aldrich, CastleHill, NSW, Australia) for 45 min. Blocking and permeabilisation was achieved by incubation with 5 % goat serum (Gibco, ThermoFisherScientific, Scoresby, VIC, Australia) and 0.1 % Triton-X100 (MerckMillipore, Bayswater, VIC, Australia) in phosphate-buffered-saline (PBS) for 2 h at room temperature. Primary antibody staining against the endothelial marker CD31 (cat no. bba7, R&D Systems; 1:200 in 1 % goat serum) was performed overnight at 4 °C. Subsequently, the samples were washed in 1 % goat serum in PBS for 8 h with three changes of the washing buffer. Polyclonal goat anti-mouse IgG conjugated to Alexa-Fluor 488 (cat no. A11001, Invitrogen, ThermoFisherScientific, Scoresby, VIC, Australia; 1:300) secondary antibody, Alexa-Fluor 633 conjugated Phalloidin (Invitrogen, ThermoFisherScientific, Scoresby, VIC, Australia; 1:100), and  $5 \mu\text{g mL}^{-1}$  4',6-diamidino-2-phenylindole (DAPI) in 1 % goat serum/PBS were applied overnight at 4 °C. Images were acquired on a Nikon A1R inverted confocal microscope (Nikon Instruments Inc.; 10x,  $1.32 \mu\text{m px}^{-1} \times 1.32 \mu\text{m px}^{-1}$ , z-step size  $2.5 \mu\text{m} \times 181$ ).

## Availability of source code and requirements

- Project name: Qiber3D
- Project home page: <https://github.com/theia-dev/Qiber3D>
- Operating system(s): Platform independent
- Programming language: Python
- Other requirements: Python  $\geq 3.7$ , for a list of required Python libraries, refer to the project's [requirements.txt](#)
- License: MIT

## Availability of supporting data and materials

The raw image of the microvascular-like network is available at <https://doi.org/10.6084/m9.figshare.13655606>.

## Declarations

### List of abbreviations

CAF Cancer-associated fibroblasts  
 CT computed tomography  
 DAPI 6-diamidino-2-phenylindole  
 ECM endothelial cell medium  
 FBS fetal bovine serum  
 FGF-2 human fibroblast growth factor 2  
 HPC high-performance computing

MPI Message Passing Interface  
 MRI Magnetic resonance imaging  
 PBS Phosphate-buffered saline  
 PFA paraformaldehyde  
 SDF-1 stromal cell-derived factor 1  
 TEASAR Tree-structure Extraction Algorithm for Accurate and Robust skeletons  
 VEGF Vascular endothelial growth factor

## Ethical Approval (optional)

All experiments involving human cells were approved by the Queensland University of Technology Human Research Ethics Committee (Approval number: 1800000502).

## Consent for publication

not applicable

## Competing Interests

The authors declare that they have no competing interests.

## Funding

AJ was supported by a Postgraduate Research Award (International), QUT. LB was supported by a grant from the National Breast Cancer Foundation (PF-16-004) and acknowledges the support of grant 1159637 awarded through the 2018 Priority-driven Collaborative Cancer Research Scheme and co-funded by Cancer Australia and Leukemia Foundation of Australia. Some of the data reported in this work were obtained at the Central Analytical Research Facility (CARF) operated by the Institute for Future Environments, QUT. Access to CARF was supported by the Science and Engineering Faculty, QUT.

## Author's Contributions

AJ performed the experiments. HE and AJ developed the toolkit. AJ and HE analyzed and interpreted the data, and wrote the manuscript. AJ, HE and LJB read, edited and approved the final manuscript.

## Acknowledgements

HE acknowledges the Duke University, Center for Autonomous Materials Design, for computational support and Prof. Stefano Curtarolo for fruitful discussions.

## References

1. Carmeliet P, Jain RK. Angiogenesis in Cancer and Other Diseases. *Nature* 2000;407(6801):249–257.
2. Staton CA, Reed MWR, Brown NJ. A Critical Analysis of Current in Vitro and in Vivo Angiogenesis Assays. *International Journal of Experimental Pathology* 2009;90(3):195–221.
3. Conchello JA, Lichtman JW. Optical Sectioning Microscopy. *Nature Methods* 2005;2(12):920–931.
4. Rytlewski JA, Geuss LR, Anyaeji CI, Lewis EW, Suggs LJ. Three-Dimensional Image Quantification as a New Morphometry Method for Tissue Engineering. *Tissue Engineering Part C, Methods* 2012;18(7):507.
5. Stalling D, Westerhoff M, Hege HC. Amira: A Highly Interactive

- System for Visual Data Analysis. In: Visualization Handbook<sup>550</sup> Elsevier; 2005.p. 749–767.
6. Peng H, Ruan Z, Long F, Simpson JH, Myers EW. V3D Enables Real-Time 3D Visualization and Quantitative Analysis of Large-Scale Biological Image Data Sets. *Nature Biotechnology* 2010;28(4):348–353.<sup>555</sup>
  7. Schindelin J, Arganda-Carreras I, Frise E, Kaynig V, Longair M, Pietzsch T, et al. Fiji: An Open-Source Platform for Biological-Image Analysis. *Nature Methods* 2012;9(7):676–682.<sup>490</sup>
  8. Fedorov A, Beichel R, Kalpathy-Cramer J, Finet J, Fillion-Robin JC, Pujol S, et al. 3D Slicer as an Image Computing Platform for the Quantitative Imaging Network. *Magnetic resonance imaging* 2012;30(9):1323–1341.
  9. Eliceiri KW, Berthold MR, Goldberg IG, Ibáñez L, Manjunath BS, Martone ME, et al. Biological Imaging Software Tools. *Nature Methods* 2012;9(7):697–710.<sup>495</sup>
  10. Lee E, Takahashi H, Pauty J, Kobayashi M, Kato K, Kabara M, et al. A 3D in Vitro Pericyte-Supported Microvessel Model: Visualisation and Quantitative Characterisation of Multistep Angiogenesis. *Journal of Materials Chemistry B* 2018;6(7):1085–1094.<sup>500</sup>
  11. Nishiguchi A, Matsusaki M, Kano MR, Nishihara H, Okano D, Asano Y, et al. In Vitro 3D Blood/Lymph-Vascularized Human Stromal Tissues for Preclinical Assays of Cancer Metastasis. *Biomaterials* 2018;179:144–155.<sup>505</sup>
  12. Bonda U, Jaeschke A, Lighterness A, Baldwin J, Werner C, De-Juan-Pardo EM, et al. 3D Quantification of Vascular-Like Structures in z Stack Confocal Images. *STAR Protocols* 2020;p. 100180.<sup>510</sup>
  13. Sato M, Bitter I, Bender MA, Kaufman AE, Nakajima M. TEASAR: Tree-Structure Extraction Algorithm for Accurate and Robust Skeletons. In: Proceedings the Eighth Pacific Conference on Computer Graphics and Applications IEEE Comput. Soc; 2000. p. 281–449.<sup>515</sup>
  14. Bitter I, Kaufman AE, Sato M. Penalized-distance volumetric skeleton algorithm. *IEEE Transactions on Visualization and Computer Graphics* 2001;7(3):195–206.
  15. Otsu N. A Threshold Selection Method from Gray-Level Histograms. *IEEE Transactions on Systems, Man, and Cybernetics* 1979;9(1):62–66.<sup>520</sup>
  16. Lee TC, Kashyap RL, Chu CN. Building Skeleton Models via 3-D Medial Surface Axis Thinning Algorithms. *CVGIP: Graphical Models and Image Processing*;56(6):462–478.<sup>525</sup>
  17. Keller LM, Holzer L, Wepf R, Gasser P. 3D geometry and topology of pore pathways in Opalinus clay: Implications for mass transport. *Applied Clay Science* 2011;52(1-2):85–95.
  18. Song Y, Davy CA, Troadec D, Blanchenet AM, Skoczylas F, Talandier J, et al. Multi-scale pore structure of COx claystone: Towards the prediction of fluid transport. *Marine and Petroleum Geology* 2015;65:63–82. Cited By 46.
  19. Evers JF, Schmitt S, Sibila M, Duch C. Progress in Functional Neuroanatomy: Precise Automatic Geometric Reconstruction of Neuronal Morphology From Confocal Image Stacks. *Journal of Neurophysiology* 2005;93(4):2331–2342.<sup>535</sup>
  20. Takemura S, Bharioke A, Lu Z, Nern A, Vitaladevuni S, Rivlin PK, et al. A visual motion detection circuit suggested by *Drosophila* connectomics. *Nature* 2013;500(7461):175–181.
  21. Musy M, Dalmaso G, Sullivan B, Marcomusy/Vtkplotter: Vtkplotter; 2019.<sup>540</sup>
  22. Jacobs B, Garcia ME, Shea-Shumsky NB, Tennison ME, Schall M, Saviano MS, et al. Comparative morphology of gigantopyramidal neurons in primary motor cortex across mammals. *Journal of Comparative Neurology* 2018;526(3):496–536.
  23. Lawrence MG, Taylor RA, Toivanen R, Pedersen J, Norden S, Pook DW, et al. A Preclinical Xenograft Model of Prostate Cancer Using Human Tumors. *Nature Protocols* 2013;8(5):836–848.<sup>545</sup>
  24. Tsurkan MV, Chwalek K, Prokoph S, Zieris A, Levental KR, Freudenberg U, et al. Defined Polymer-Peptide Conjugates to Form Cell-Instructive starPEG-Heparin Matrices In Situ. *Advanced Materials* 2013;25(18):2606–2610.
  25. Bray LJ, Binner M, Holzheu A, Friedrichs J, Freudenberg U, Huttmacher DW, et al. Multi-Parametric Hydrogels Support 3D in Vitro Bioengineered Microenvironment Models of Tumour Angiogenesis. *Biomaterials* 2015;53:609–620.



Click here to access/download  
**Supplementary Material**  
2020\_Qiber3D\_suppl.pdf

